Published in final edited form as:
Nat Methods. 2016 August ; 13(8): 661–664. doi:10.1038/nmeth.3897.

Varying label density allows artifact-free analysis of membrane-protein nanoclusters

Florian Baumgart[*,1], **Andreas Arnold**[1], **Konrad Leskovar**[1], **Kaj Staszek**[1], **Martin Fölser**[1], **Julian Weghuber**[2], **Hannes Stockinger**[3], and **Gerhard. J. Schütz**[*,1]

[1]Institute of Applied Physics, TU Wien, Vienna, Austria

[2]School of Engineering and Environmental Sciences, University of Applied Sciences Upper Austria, Wels, Austria

[3]Institute for Hygiene and Applied Immunology, Medical University of Vienna, Vienna, Austria

Abstract

We present a new method to robustly discriminate clustered from random distributions of molecules detected with single molecule localization microscopy-based techniques like PALM and STORM. The approach is based on the deliberate variation of the labeling density, e.g. by titration of fluorescent antibody, combined with quantitative cluster analysis. It thereby circumvents the problem of cluster artifacts generated by overcounting of blinking fluorophores.

In recent years, several strategies have been developed to achieve nanoscopic resolution in light microscopy. Among them, single molecule localization-based methods including photo-activated localization microscopy (PALM) and (direct) stochastic reconstruction microscopy ((d)STORM) have become increasingly popular1. The techniques rely on fluorophores that can be stochastically switched between a dark off- and a fluorescent on-state under conditions where only a marginal number of fluorophores is in the on-state at any given time. Typically, stacks of thousands of images are recorded from a sample that is chemically fixed to prevent motion of the fluorophores during data acquisition. Finally, single molecule positions are determined2 and localization maps of the sampled molecules are reconstructed. Currently, a number of image processing algorithms are available to identify and characterize clusters of single molecule localizations3–7.

[*]correspondence should be addressed to Florian Baumgart (baumgart@iap.tuwien.ac.at) or Gerhard J. Schütz (schuetz@iap.tuwien.ac.at).

Author contributions

F.B., K.L., A.A. and K.S. performed experiments; F.B. analyzed the data; A.A. and K.L. wrote the code for the analytical methods; A.A. wrote the code for the simulations; M.F. implemented Ripley's K analysis; H.S. and J. W. provided cell lines and materials; F.B., A.A. and G.J.S. developed the analytical method and conceived the simulations; F.B. and G.J.S. wrote the manuscript.

Competing financial interests

The authors declare no competing financial interests.

Code availability. We provide the code used for data analysis as Matlab files. See Supplementary Software for details.

Europe PMC Funders Author Manuscripts

In the field of membrane biology, PALM and (d)STORM have been widely used, providing maps of plasma membrane constituents or associated proteins in unprecedented detail1, 5, 8–12. One remarkable finding has been the observation of nanoscale clustering of virtually any membrane protein8. Recently, however, notes of caution were raised that multiple observations of single fluorophores also lead to clustered localizations and may closely resemble clustered molecules3, 13–17, thereby impairing direct conclusions from the observed localization clusters on the presence of protein clusters. The main problem arises from the stochastic blinking behavior of organic fluorophores as well as fluorescent proteins.

Several researchers have approached this problem by *a posteriori* methods. Annibale et al proposed to combine events that are assumed to be caused by multiple observations of the same fluorophore3, 14. This approach, however, is hampered by the difficulty to discriminate overcounting of the same dye molecule from observations of different colocalized dye molecules, especially when long-lived dark states of fluorophores are present3. Another method applies pair (auto-) correlation analysis (PCA) to address the problem of overcounting5. A PCA curve ideally consists of two more or less well separated components: a short decay corresponding to multiple observations of the same dye molecules within the localization precision, and a long decay reporting the size of true protein clusters. Provided that all molecules are immobilized, PCA is robust against heterogeneities in the dye blinking statistics. Chemical fixation protocols, however, are often insufficient to completely immobilize the molecular components of cellular samples18, particularly in view of the long recording times of tens of minutes required for obtaining superresolution images. In addition, the method reaches its limits when protein clusters are not significantly larger than the spread of localizations obtained from a single blinking fluorophore.

In contrast to previous approaches based on post-processing, we tried to find experimental criteria to distinguish random from clustered distributions of molecules, which are insensitive to the blinking statistics of the used fluorophores and their residual mobility. We reasoned that varying the labeling density would lead to characteristic changes in the obtained localization maps. For homogeneous protein distributions the relative area covered by apparent clusters resulting from fluorophore blinking will increase steadily with increasing degree of labeling. Concurrently, the density of localizations per cluster will remain constant. Conversely, if molecules are clustered the relative area will saturate, and the density of localizations per cluster will be proportional to the degree of labeling.

In order to test our predictions, we simulated localization maps for randomly distributed (Fig. 1a) and clustered (Fig. 1b) molecules at varying density. Each molecule was allowed to blink stochastically, yielding an average of seven observations per molecule that were distributed around each molecular position with a localization error of 40 nm. Clusters were simulated by randomly distributing varying numbers of molecules within circles with a radius of 50 nm, which corresponds to the size of published nanoclusters10. Notably, irrespective whether randomly distributed or clustered molecules were simulated, all images display heterogeneities in the localization density, which is also reflected by characteristic peaks in Ripley’s K function (Supplementary Fig. 1). Our method is based on the quantitative characterization of these apparent clusters at different labeling densities. Binary

cluster masks were established from thresholded localization density maps based on the recorded or simulated single molecule positions and the known localization errors (Fig. 1a and b; see also Methods and Supplementary Fig. 2). For each image, we counted the number of total localizations per μm^2 (locs/μm^2), the relative area coverage by the cluster masks (η), and the average density of localizations within the apparent clusters (ρ). Both η and ρ showed a characteristic difference in their dependence on locs/μm^2 for randomly distributed versus truly clustered molecules (Fig. 1c). We defined the intersection of the density curves with the y-axis as ρ_0; hence, $\rho_0 \cdot \sigma^2 \pi$ gives an estimate of the number of counted localizations per molecule, with σ denoting the localization precision. The difference between clustered and random distributions becomes even more pronounced when plotting the normalized density ρ/ρ_0 against η: for randomly distributed molecules a rather horizontal line can be observed, whereas true clustering yields a strong increase in ρ/ρ_0.

In order to validate the robustness of our approach, we varied several parameters in our simulations. First, we ensured that the selected threshold for the mask algorithm and the degree of overcounting had no effect on the results of the analysis; the latter accounts for multiple reappearances of single dye molecules and for the presence of multiple chromophores per labeling antibody. Both for randomly distributed and for clustered data we obtained robust curves after normalization (Supplementary Fig. 3a and b; see Supplementary Fig. 3c-f for not-normalized curves). Also residual mobility of the randomly distributed proteins had no effect on the shape of the obtained curves (Supplementary Fig. 4a and b). As discussed above, repeated photoactivation cycles of the same molecule generate pseudo-clusters in superresolution images which are difficult to discriminate from true clusters. We thus simulated the worst case scenario, in which a small proportion of randomly distributed molecules is virtually not photobleachable and thus generates substantially more localizations per molecule than the average (Supplementary Fig. 4c and d). Also under these circumstances, the overall shape of the curve remained unchanged. The additional spread in the ρ/ρ_0 ratios for small values of η can be ascribed to fluctuations in the total number of non-bleachable molecules per localization map. Taken together, we could use the obtained η-dependence of ρ/ρ_0 for randomly distributed localizations as a reference curve for subsequent plots (red line plotted in Fig. 1c).

We next evaluated the effect of different numbers of true clusters per image (Supplementary Fig. 4e) and of different cluster sizes (Supplementary Fig. 4f). From this it becomes evident that our approach robustly detects a broad range of cluster scenarios; only high numbers and large sizes of clusters are difficult to identify, as the images converge to a homogeneous distribution of localizations. Next, we emulated the effect of the presence of non-clustered molecules or of unspecifically bound label by adding randomly distributed blinking molecules to our clustered localization maps. The presence of large numbers of background signals shifted the obtained curves towards the reference for randomly distributed molecules (Supplementary Fig. 4g). In summary, our method yields clear differences between random and clustered distributions of molecules over a broad range of cluster parameters.

We further assessed the sensitivity of our method to detect small oligomers. To this end, we simulated pentamers at a density of 50 molecules per μm^2 (i.e. 10 pentamers per μm^2). We further included free monomers at varying concentrations up to equal densities as

background. To mimic the label titration experiment, we calculated images with increasing numbers of dye molecules assigned to each oligomer. As expected, increasing background levels of unclustered molecules reduced the sensitivity (Supplementary Fig. 4h). Still, our simulation shows that pentamers can be readily detected at all simulated background levels.

Having tested our method on simulated data, we further evaluated our approach in a synthetic experimental setting. We used microcontact printing to produce circular clusters of IgG arranged in periodic patterns on glass surfaces (~200 nm diameter, ~6 clusters per μm^2); interspaces were passivated by BSA. To mimic random protein distributions, we immobilized the biotinylated primary IgG via streptavidin randomly on the glass surface. In both cases, an AF647-conjugated secondary antibody was titrated to probe for clustering. Imaging conditions, particularly laser settings, were kept constant for recording the titration series. The ρ/ρ_0 versus η plot shows clear differences between the clustered scenario and the random distribution (Fig. 2).

Finally, we applied our method in cell biological settings. Clathrin-coated pits (CCPs) represent a well-established example for protein clusters in the plasma membrane19. We stained CCPs in fixed Jurkat cells with different concentrations of an AF647-labeled clathrin-heavy chain- (HC-) specific antibody (Supplementary Fig. 5a), thereby varying the degree of clathrin labeling between ~5% and ~85% (Supplementary Fig. 6a). Indeed, results were characteristic for clustered molecules (Fig. 3a).

To test our method on membrane protein nanodomains, we analyzed the clustering of LFA-1, an integrin specific to immune cells, which was reported to cluster upon activation20. Also in this case, we found pronounced deviation from a random distribution (Fig. 3b and Supplementary Fig. 6b). As negative control, we confirmed previous PALM data5 that glycosylphosphatidylinositol- (GPI-) anchored mGFP does not form substantial clusters in the plasma membrane (Fig. 3c and Supplementary Fig. 6c). In this case, we titrated AF647-labeled GFP-Trap to detect the mGFP-GPI.

The major asset of our method, however, is its robustness against the erroneous detection of nanoclusters due to overcounting. Specifically, several reports have proposed the existence of nanoscopic clusters of signaling components in T cells4, 9, 10. One example relates to Lck, the key kinase responsible for early T cell signaling, which was found to be clustered in domains of 100 nm diameter10. We hence used our method to revisit Lck nanoclustering on the T cell plasma membrane. At first inspection, dSTORM data of endogenous Lck labeled with an AF647-conjugated antibody might seem indicative of a non-random protein distribution (Supplementary Fig. 5b). Label titration analysis, however, yielded results consistent with a homogeneous protein distribution, and hence did not support the presence of Lck nanoclusters (Fig. 3d and Supplementary Fig. 6d).

If nanocluster formation does not directly depend on the protein of interest, our method is also compatible with PALM by using natural variations in the expression levels between individual cells. For this, we analyzed the clustering behavior of ectopically overexpressed GPI-anchored mEOS3.2, and an mEOS3.2-chimera of Lck. Consistent with the dSTORM experiments, we found considerable heterogeneity in the single molecule localizations

(Supplementary Fig. 7), but no clustering of the two constructs (Fig. 3e and f). In the case of Lck, also T cell activation via antibody-coated surfaces did not affect the random distribution (Supplementary Fig. 8). Finally, we reconstructed the putative diffraction-limited image from an Lck-mEOS3.2 superresolution image and compared it with the according diffraction-limited protein distribution obtained by direct antibody labeling of Lck-mEOS3.2 on the very same cell; strikingly, there was no similarity between the two images (Supplementary Fig. 7), thereby demonstrating the extent of the problem.

In summary, our method complements current experimental strategies to characterize protein organization at the nano-scale. It can detect nanoclustering over a broad range of parameters found in cells. Importantly, the approach is insensitive to common imaging artifacts inherent to single molecule localization-based superresolution techniques.

Online Methods

Cell culture, DNA constructs, antibodies and reagents

Jurkat E6-1 T cells and Chinese Hamster Ovary (CHO) cells were from the American Type Culture Collection. Lck-deficient JCaM1.6 T cells were from the European Collection of Authenticated Cell Cultures. All cell lines were regularly tested to exclude *Mycoplasma* contamination. Jurkat cell lines were cultured in RPMI 1640 medium (Sigma-Aldrich), CHO cells in DMEM/HAM's F-12 medium (Lonza); media were supplemented with 10% fetal bovine serum (FBS), 2 mM L-glutamine, 1,000 U ml^{-1} penicillin/streptomycin (all from Sigma-Aldrich) and cells were grown in a humidified atmosphere at 37 °C and 5% CO_2. For microscopy, we used an imaging buffer consisting of HBSS (Lonza) supplemented with 2% FBS. Fluorescent proteins (mEOS3.2, mGFP) were fused to the C-terminus of Lck21 or to the N-terminus of the GPI-anchor signal of the human folate receptor22. Fusion proteins were obtained by site-specifically inserting the PCR amplified sequence of the respective fluorescent protein into the retroviral expression vector construct pBMN-Z-Lck. Stable cell lines were generated by retroviral infections based on protocols from G. Nolan (Stanford University). Positive cells were enriched via a fluorescence assisted cell sorter (FACSAria; BD Biosciences). Fura-2-AM was from Molecular Probes. Cholesterol-PEG-KK114 was provided by A. Honigmann (Max Planck Institute of Molecular Cell Biology and Genetics, Dresden). Lck-specific antibody (BioLegend; clone Lck-01; catalog number 628301), LFA-1 (CD11)-specific antibody (BioLegend; clone TS2/4; catalog number 350602) and GFP-Trap (ChromoTek) were labeled with Alexa Fluor (AF) 647-NHS (Molecular Probes) following the supplier's instructions and purified with Zeba desalting columns (Thermo Fisher Scientific). AF647-labeled antibody (clone X22) against clathrin heavy chain (anti-clathrin-HC-AF647) was purchased from Novus Biologicals (catalog number NB300-613AF647). CD3ε-specific antibody (clone OKT3; catalog number SAB4700041), fibronectin for surface coating and all other chemicals were obtained from Sigma-Aldrich if not noted otherwise. The biotinylated murine GFP-antibody (clone 9F9.F9; catalog number NB110-40670) was purchased from Novus Biologicals, AF647-conjugated goat anti-mouse secondary antibody was from Thermo Fisher Scientific (catalog number A-21235).

Sample preparation

For imaging, cells were seeded on surface-coated LabTek chamber slides in imaging buffer at 37 °C for 5-10 min. Surfaces were prepared by incubating slides with 50 μg ml^{-1} fibronectin for 30 min at RT. To activate Jurkat cells, slides were coated with 10 μg ml^{-1} anti-CD3ε for 2 hrs at 37 °C. For experiments under activating conditions, cells were incubated on anti-CD3ε-coated glass slides for 10 min at 37 °C. Cells were fixed with 4% paraformaldehyde (PFA) for 10 min at RT. For antibody staining, cells were permeabilized with 0.1% (wt/vol) Triton X-100 for 10 min at RT and unspecific binding sites were blocked by incubation with blocking buffer consisting of HBSS containing 5% BSA (wt/vol) for 30 min at RT. Samples were incubated with antibodies diluted in blocking buffer at varying concentrations for 2 hrs at RT. Finally, cells were washed with HBSS and fixed again with 4% PFA for 10 min at RT to avoid unbinding of antibodies during dSTORM measurements23.

Soft Lithography

Microstructured surfaces were made following a protocol adapted from Schwarzenbacher et al.24. Polydimethylsiloxan- (PDMS-) based polymers with 200 nm pillars (EV Group) were incubated with 50 μg ml^{-1} streptavidin in PBS for 15 min and dried with N_2. Immediately after drying, the stamp was placed onto a plasma-cleaned glass coverslip (Menzel Gläser, Cover Slips #1) and incubated for 60 min. After removal of the stamp, the coverslip was incubated with biotinylated mouse IgG for 15 min at a concentration of 10 μg ml^{-1} in PBS with 1% BSA (wt/vol) and washed extensively with PBS. Finally, AF647-conjugated goat anti-mouse antibody was titrated at different concentrations, incubated for 15 min and washed with PBS. All steps were performed at RT.

Microscopy setup

All experiments were performed on a modified Zeiss Axiovert 200 inverted microscope equipped with a 100 × oil-immersion objective (Zeiss Apochromat NA1.46). The setup was equipped with a 640 nm diode laser (Toptica iBeam smart 200 mW), a 532 nm diode-pumped solid state (DPSS) laser (Spectra physics Millennia 6s) and a near UV light 405 nm ion laser (Coherent Innova 90C). Intensity modulation and timings were controlled either directly or with an acousto-optic modulator (AOM) using custom-written Labview software. Laser lines were overlaid with an OBIS Galaxy beam combiner (Coherent). Emission light was filtered using appropriate filter sets (Chroma) and recorded on an IXON DU 897-DV EM-CCD camera (Andor). Multi-color imaging was performed using an emission light splitter (Optosplit; Cairn Research) adapted to the spectral characteristics of the used fluorophores. Total internal reflection fluorescence (TIRF) illumination was achieved by shifting the excitation beam in parallel to the optical axis with a mirror mounted on a motorized movable table. For ratiometric Fura-2 imaging, we used a polychromatic Xenon light source combined with a monochromator (polychrome V; TILL photonics) that provided light at 340 nm and 380 nm.

Ratiometric Ca^{2+} measurements

T cell activation was quantified with Fura-2-AM. Cells were incubated with 5 μg ml^{-1} Fura-2-AM in supplemented RPMI medium for 15 min at RT, washed twice in imaging buffer and kept on ice until imaging. For each experiment, cells were resuspended in imaging buffer at 5×10^7 cells/ml and 5 μl were deposited close to the surface of an imaging chamber, which was mounted on the microscope at RT. Image acquisition began immediately, recording 1,000 frames at 1 Hz. Image stacks were processed and analyzed using ImageJ.

Quantitative antibody binding assay

In order to quantify the degree of antibody binding, we labeled fixed and permeabilized cells labeled with different concentrations of AF647-conjugated antibodies. Antibody binding was measured as mean fluorescence per pixel under TIRF illumination using the 640 nm laser line. For each dilution step 15-20 cells were imaged. Average background-corrected fluorescence values were fitted to the equation $[AB] = [B] \cdot [A_{max}] / (K_d + [B])$ assuming first order binding, where [AB] denotes the surface density of bound antibody, [B] is the antibody concentration in solution, $[A_{max}]$ stands for the fitted total surface density of antibody binding sites and K_d is the dissociation constant.

Superresolution microscopy and image reconstruction

PALM experiments were carried out in imaging buffer. For excitation of mEOS3.2 we used the 532 nm laser line. The 405 nm laser constantly illuminated the sample in order to continuously switch new molecules. For dSTORM measurements, we used previously published switching buffer conditions optimized for AF64723: PBS (pH 7.4) was supplemented with 10% glucose, 0.5 mg ml^{-1} glucose oxidase, 40 μg ml^{-1} catalase and 50 mM cysteamine. In dSTORM experiments with AF647, the majority of fluorophores was first transferred into a non-fluorescent dark state using high power 640 nm laser illumination. Then, single molecules were imaged at 640 nm excitation at lower power, keeping the 405 nm laser continuously on in order to switch molecules back to a fluorescent state. Both PALM and dSTORM images were recorded as stacks of 10,000 frames at 100 Hz. Stroboscopic illumination protocols were applied with 3 ms illumination time and 7 ms delay between consecutive images. Single molecule signal localization and image reconstruction was carried out with the open-source ImageJ plugin ThunderSTORM25. Stringent post-processing parameters were chosen to discard signals with low localization precision. On average, we obtained localization errors of σ = 20 nm for AF647 and σ = 30 nm for mEOS3.2. Merging of localizations was performed with a grouping radius adjusted to the average localization precision of the respective fluorophores. If not specified otherwise, we used 50 frames off-time. No drift correction was applied. Ripley's K analysis26 was carried out using custom-written Matlab code.

Quantitative cluster analysis

Clusters were identified using custom-written Matlab code (Supplementary Software). Each localization within a region of interest was represented by a 2D Gaussian function with fixed σ = 35 nm, centered at the recorded position. By summing up the Gaussian peaks,

localizations in close proximity to each other resulted in higher peaks than well separated localizations (Supplementary Fig. 2a). Binary cluster masks were obtained by applying a threshold (thr = 2.5) that was chosen after visual inspection of cluster masks at different thresholds (Supplementary Fig. 2c). The cluster masks were then used to classify localizations as clustered or not-clustered. To reduce the overestimation of cluster sizes, 2D Gaussians were set to zero beyond a radius of 2σ (Supplementary Fig. 2b). Finally, the total cluster area (A_{in}) within the region of interest (A), as well as the number of localizations inside ($\#_{in}$) and outside of clusters ($\#_{out}$) was determined. This allowed us to calculate the density of localizations per cluster area ($\rho = \#_{in}/A_{in}$) and the relative clustered area per image ($\eta = A_{in}/A$).

Simulation of randomly distributed molecules

Molecules were distributed randomly as xy coordinates on a 12,800 × 12,800 nm sized image. Each molecule was assumed to yield multiple localizations due to blinking with an average of seven observations per molecule drawn from an exponential distribution. Localizations were scattered around the xy position of each molecule, following a 2D Gaussian probability distribution defined by σ = 40 nm. To account for variations in the labeling density, we simulated different numbers of molecules over a broad range, keeping all other parameters constant. Random noise consisting of 300 randomly distributed single localizations was also included in each image. In Supplementary Figure 3, we varied the blinking statistics and the analysis threshold. In Supplementary Figure 4a and b, we tested the effect of residual diffusion of molecules during image acquisition. To simulate single molecule trajectories, we assumed a diffusion coefficient $D = 1.1 \times 10^{-5}$ μm² s^{-1} (determined experimentally for Lck-mEOS3.2 in fixed JCaM1.6 cells, not shown) as well as a specified image acquisition rate and total number of recorded frames. Localizations were then randomly distributed along each trajectory, using the blinking statistics and the localization errors as above. Finally, in Supplementary Figure 4c and d we included the indicated small fractions of molecules with different blinking statistics of 100 localizations per molecule on average (exponentially distributed).

Determination of the standard curve for randomly distributed localizations and ρ_0

We simulated data for randomly distributed molecules under different conditions (variations in blinking statistics and thresholds, see Supplementary Figure 3). Each data set could be fitted well with a polynomial of the form $\rho = \rho_0(1 + \alpha \cdot \eta^b)$ with constant $\alpha = 1.4$ and $b = 4$; ρ_0 turned out to depend on various imaging and analysis parameters. We normalized the data sets with respect to ρ_0, yielding the average reference curve for randomly distributed localizations $\rho/\rho_0 = 1 + 1.4 \cdot \eta^4$. Clustered distributions could also be fitted well with this polynomial, albeit with different values for α and b. We hence used such fits for determining ρ_0 in all simulations and experiments, which ultimately allowed for plotting ρ/ρ_0 versus η.

Simulation of clustered molecules

To simulate clusters, molecules were placed randomly according to a uniform distribution within circles around cluster centers, which themselves were distributed uniformly within the field of view. The number of molecules per cluster was varied following a normal distribution with a standard deviation of 33% of the mean number of molecules per cluster.

Additionally, we added molecules that were uniformly distributed over the whole field of view (25% of the total number of clustered molecules), in order to account for unspecific binders or monomeric blinking molecules. All simulated molecules followed the same blinking statistics (average of seven localizations per molecule). Random noise consisting of 300 uniformly distributed single localizations was further included in each image. In order to account for variations in the labeling density, we simulated different numbers of molecules per cluster over a broad range, keeping all other parameters constant.

Simulation of pentamers

Pentamers were simulated as randomly distributed 5-mer centers. Each pentamer center was filled with n molecules following a binomial distribution with the probability p. Hence, p corresponds to the labeling efficiency in a titration experiment. As in the other simulations, each molecule was assumed to yield multiple localizations due to blinking with an average of seven observations per molecule drawn from an exponential distribution. Random noise consisting of 300 randomly distributed single localizations was also included in each image. Additionally, we added different amounts of molecules that were uniformly distributed over the whole field of view, in order to account for unspecific binders or monomeric blinking molecules. For all simulations of small oligomers, the total number of molecules was kept constant (50 μm^{-2}), only p was varied.

Supplementary Material

Refer to Web version on PubMed Central for supplementary material.

Acknowledgements

This work was supported by the Austrian Science Fund (FWF projects P 26337-B21 (G.J.S.), P 25730-B21 (G.J.S.), W1250-B20 (G.J.S.) and P 27941-E28 (F.B.)), and by the Austrian Research Promotion Agency (FFG project number 842379 (J.W.)). We would like to thank J. Huppa for critical reading of the manuscript and helpful comments throughout this study. We are further grateful to members of the Huppa, Stockinger and Schütz labs for valuable discussions. We acknowledge E. Parkinson and C. Donner for support with cell culture and cell sorting. We acknowledge G. Nolan (Stanford University) for originally providing retroviral plasmids (pBMN-Z and helper plasmids). A. Honigmann (Max Planck Institute of Molecular Cell Biology and Genetics, Dresden) provided fluorescently labeled cholesterol (chol-PEG-KK114).

References

1. Sauer M. Localization microscopy coming of age: from concepts to biological impact. J Cell Sci. 2013; 126:3505–3513. [PubMed: 23950110]
2. Sage D, et al. Quantitative evaluation of software packages for single-molecule localization microscopy. Nat Methods. 2015; 12:717–724. [PubMed: 26076424]
3. Annibale P, Scarselli M, Kodiyan A, Radenovic A. Photoactivatable Fluorescent Protein mEos2 Displays Repeated Photoactivation after a Long-Lived Dark State in the Red Photoconverted Form. J Phys Chem Let. 2010; 1:1506–1510.
4. Rubin-Delanchy P, et al. Bayesian cluster identification in single-molecule localization microscopy data. Nat Methods. 2015; 12:1072–1076. [PubMed: 26436479]
5. Sengupta P, et al. Probing protein heterogeneity in the plasma membrane using PALM and pair correlation analysis. Nat Methods. 2011; 8:969–975. [PubMed: 21926998]
6. Fricke F, Beaudouin J, Eils R, Heilemann M. One, two or three? Probing the stoichiometry of membrane proteins by single-molecule localization microscopy. Sci Rep. 2015; 5:14072. [PubMed: 26358640]

7. Levet F, et al. SR-Tesseler: a method to segment and quantify localization-based super-resolution microscopy data. Nat Methods. 2015; 12:1065–1071. [PubMed: 26344046]
8. Garcia-Parajo MF, Cambi A, Torreno-Pina JA, Thompson N, Jacobson K. Nanoclustering as a dominant feature of plasma membrane organization. J Cell Sci. 2014; 127:4995–5005. [PubMed: 25453114]
9. Lillemeier BF, et al. TCR and Lat are expressed on separate protein islands on T cell membranes and concatenate during activation. Nat Immunol. 2010; 11:90–96. [PubMed: 20010844]
10. Rossy J, Owen DM, Williamson DJ, Yang Z, Gaus K. Conformational states of the kinase Lck regulate clustering in early T cell signaling. Nat Immunol. 2013; 14:82–89. [PubMed: 23202272]
11. Sherman E, et al. Functional nanoscale organization of signaling molecules downstream of the T cell antigen receptor. Immunity. 2011; 35:705–720. [PubMed: 22055681]
12. Ehmann N, et al. Quantitative super-resolution imaging of Bruchpilot distinguishes active zone states. Nat Commun. 2014; 5
13. Annibale P, Vanni S, Scarselli M, Rothlisberger U, Radenovic A. Identification of clustering artifacts in photoactivated localization microscopy. Nat Methods. 2011; 8:527–528. [PubMed: 21666669]
14. Annibale P, Vanni S, Scarselli M, Rothlisberger U, Radenovic A. Quantitative photo activated localization microscopy: unraveling the effects of photoblinking. PLoS One. 2011; 6:e22678. [PubMed: 21818365]
15. Whelan DR, Bell TDM. Image artifacts in Single Molecule Localization Microscopy: why optimization of sample preparation protocols matters. Sci Rep. 2015; 5:7924. [PubMed: 25603780]
16. Burgert A, Letschert S, Doose S, Sauer M. Artifacts in single-molecule localization microscopy. Histochem Cell Biol. 2015; 144:123–131. [PubMed: 26138928]
17. Sengupta P, et al. Probing protein heterogeneity in the plasma membrane using PALM and pair correlation analysis. Nat Methods. 2011; 8:969–975. [PubMed: 21926998]
18. Tanaka KAK, et al. Membrane molecules mobile even after chemical fixation. Nat Methods. 2010; 7:865–866. [PubMed: 20881966]
19. Sochacki KA, Shtengel G, van Engelenburg SB, Hess HF, Taraska JW. Correlative super-resolution fluorescence and metal-replica transmission electron microscopy. Nat Methods. 2014; 11:305–308. [PubMed: 24464288]
20. Cambi A, et al. Organization of the integrin LFA-1 in nanoclusters regulates its activity. Mol Biol Cell. 2006; 17:4270–4281. [PubMed: 16855029]
21. Paster W, et al. Genetically encoded Forster resonance energy transfer sensors for the conformation of the Src family kinase Lck. J Immunol. 2009; 182:2160–2167. [PubMed: 19201869]
22. Brameshuber M, et al. Imaging of Mobile Long-lived Nanoplatforms in the Live Cell Plasma Membrane. J Biol Chem. 2010; 285:41765–41771. [PubMed: 20966075]
23. van de Linde S, et al. Direct stochastic optical reconstruction microscopy with standard fluorescent probes. Nat Protoc. 2012; 6:991–1009.
24. Schwarzenbacher M, et al. Micropatterning for quantitative analysis of protein-protein interactions in living cells. Nat Methods. 2008; 5:1053–1060. [PubMed: 18997782]
25. Ovesný M, Křížek P, Borkovec J, Švindrych Z, Hagen GM. ThunderSTORM: a comprehensive ImageJ plugin for PALM and STORM data analysis and super-resolution imaging. Bioinformatics. 2014; 30:2389–2390. [PubMed: 24771516]
26. Ripley BD. Modeling Spatial Patterns. J Roy Stat Soc B Met. 1977; 39:172–212.

Europe PMC Funders Author Manuscripts

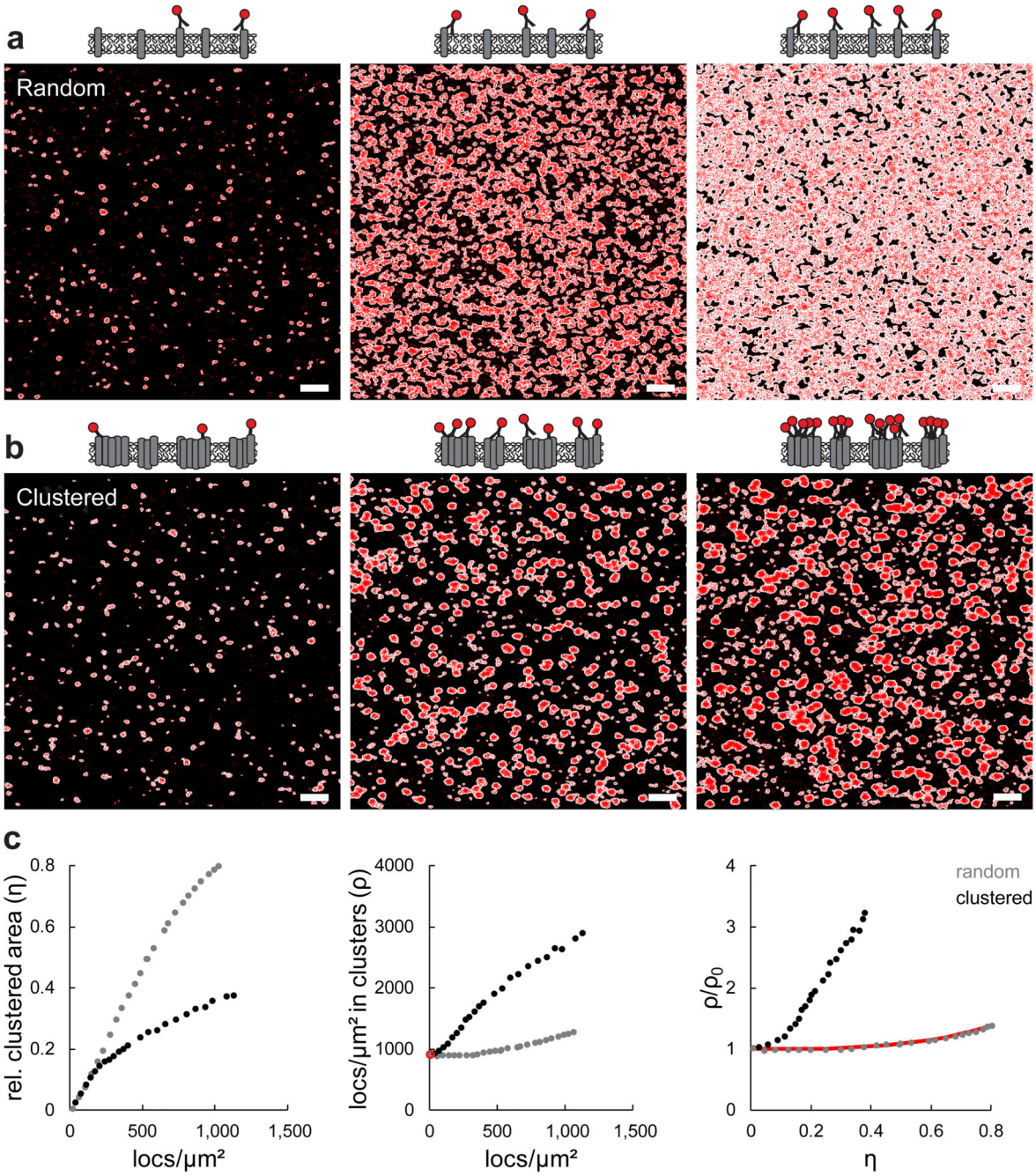

Figure 1. Effect of label density variation on randomly distributed versus clustered molecules.

(**a, b**) Simulations of increasing numbers of randomly distributed (**a**) and clustered molecules (**b**), each yielding an average of seven localizations per molecule (red); the calculated cluster masks are shown in white. For clustered distributions we assumed cluster radii of 50 nm and 3 clusters/µm^2. We simulated localization densities of ˜50 locs/µm² (left), ˜500 locs/µm² (center) and ˜1,000 locs/µm² (right). Scale bars correspond to 1 µm. (**c**) Quantification of the relative clustered area per image (η) and the density of localizations per clustered area (ρ); the plots show characteristic changes of η and ρ with increasing

numbers of localizations (left and center), as well as a characteristic η-dependence of ρ/ρ_0 (right). ρ_0, which is used for normalization of ρ/η plots, is highlighted by a red circle (center). The red line indicates the reference curve for a random distribution.

Europe PMC Funders Author Manuscripts

Europe PMC Funders Author Manuscripts

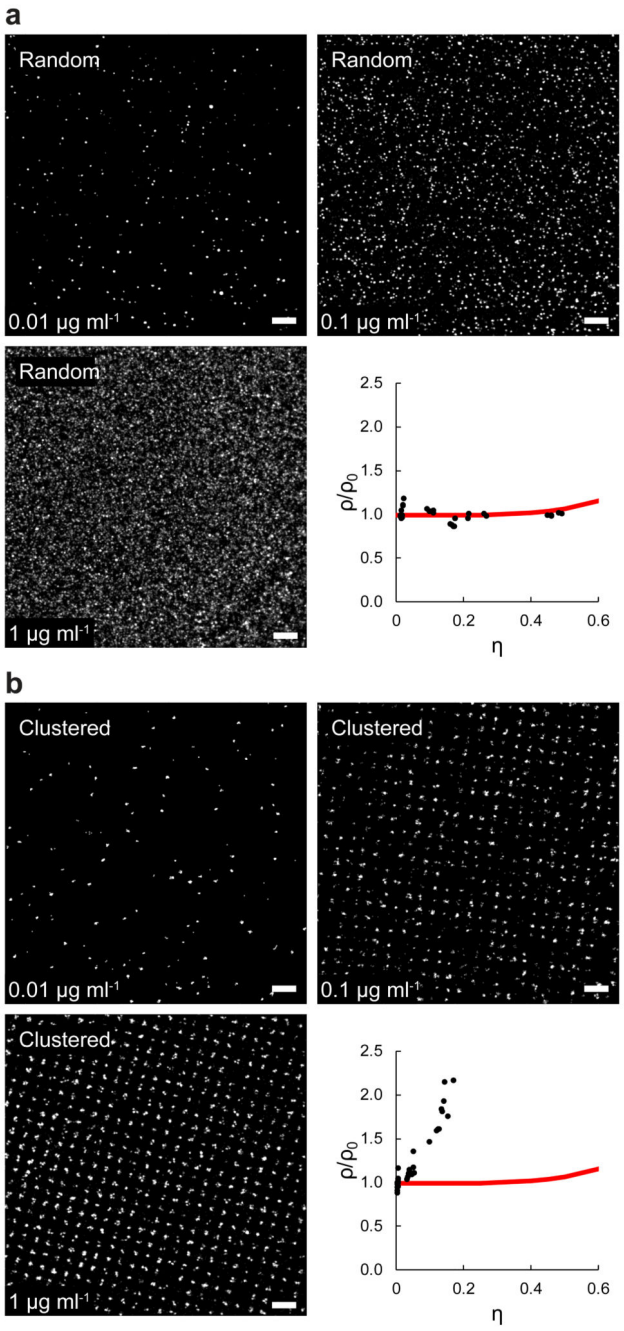

Figure 2. Label density variation of randomly distributed and clustered proteins on synthetic surfaces.

Streptavidin was adsorbed to glass surfaces either randomly (**a**) or as 200 nm-sized clusters via microcontact printing (**b**), and incubated with biotinylated murine IgG. The images show a titration series where the biotinylated IgG was detected via an AF647-conjugated IgG-specific antibody at the indicated concentrations. From reconstructed dSTORM localization maps ρ and η values were calculated for each image to generate normalized ρ/η plot (**a**, **b** bottom right, respectively). >10 images were recorded per titration step; each data point

represents a single image. The red lines indicate the reference curve for a random distribution. Scale bars correspond to 1 μm.

Europe PMC Funders Author Manuscripts

Europe PMC Funders Author Manuscripts

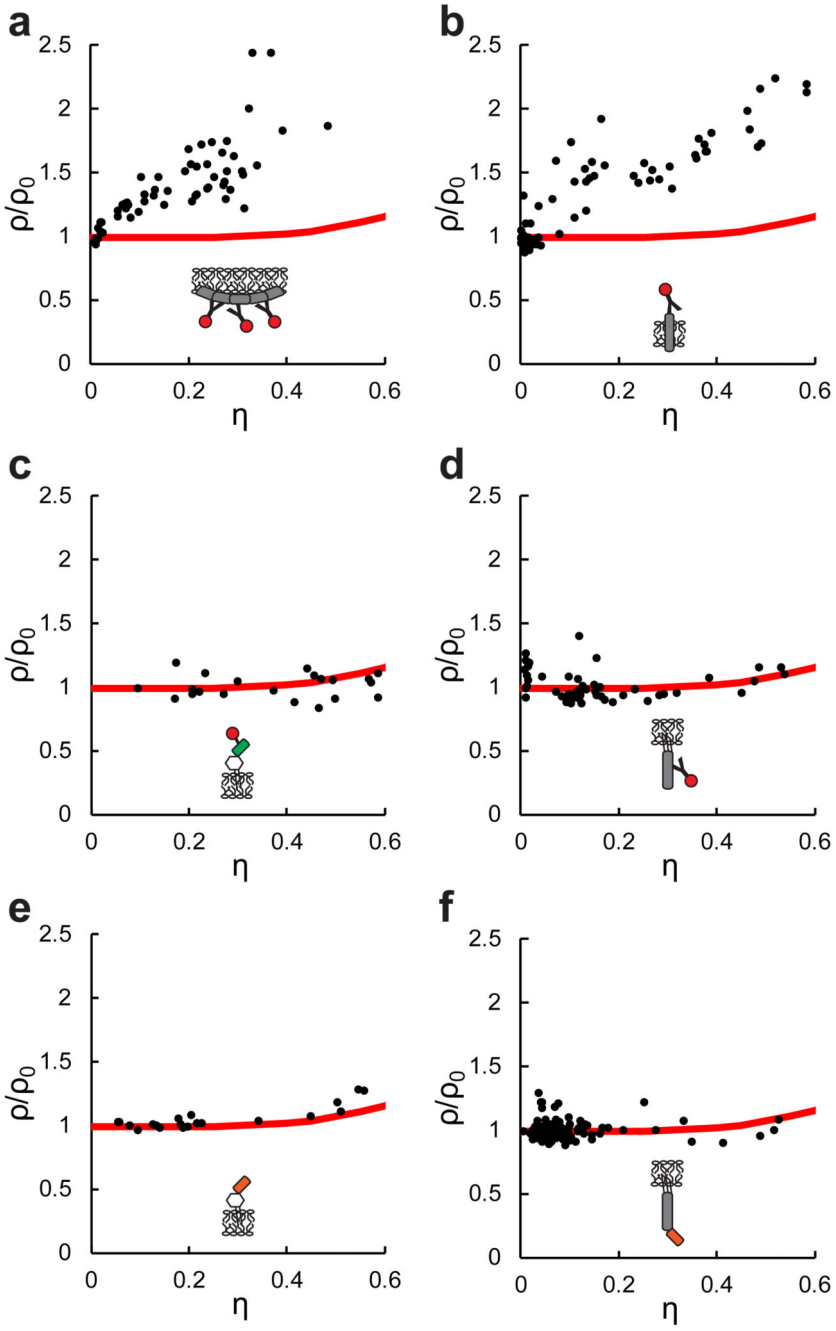

Figure 3. Cluster analysis of different proteins in the cellular plasma membrane.

Label density variation for different membrane proteins yielded characteristic normalized ρ/η curves for each protein. (**a-d**) Cells were stained at different label concentrations and imaged via dSTORM: Jurkat T cells were labeled with anti-clathrin-HC-AF647 (**a**) or anti-LFA-1-AF647 (**b**). CHO cells expressing GPI-mGFP were labeled with GFP-Trap-AF647 (**c**). Jurkat T cells were labeled with anti-Lck-AF647 (**d**). (**e**, **f**) PALM was carried out at different expression levels of GPI-mEOS3.2 in CHO cells (**e**) or Lck-mEOS3.2 in JCaM1.6

T cells (**f**). Each data point represents a single cell; up to 5 independent experiments were pooled for each graph. The red lines indicate the reference curve for a random distribution.

Europe PMC Funders Author Manuscripts